Characteristics of oblique shock waves produced in an expanding laser plasma

Tong-Nyong Lee
Optical Sciences Division, Naval Research Laboratory, Washington, D.C. 20375
(Received 12 August 1982; revised manuscript received 28 October 1982)

Stationary oblique shock waves produced by a laser-produced plasma (carbon and lithium) expanding over a wedge and related phenomena have been investigated experimentally. Such a plasma is characterized as an ionization-frozen multicomponent flow which consists of a number of different charge-state groups with different flow velocities. Well-defined multiple shock fronts which are formed around a wedge are differentiated using a spectroheliographic method. Data obtained from an ion-charge collector and from spectroheliographs indicate that these shock fronts (with different inclinations) result from different flow components. The plasma behind the shock is predominantly recombining rather than ionizing. In addition, the innermost shock is found to be more like a transverse shock where the flow particles are transported along the shock plane. This is also evidenced by a large charged-particle cumulation (and collimation) which occurs when two such oblique shock waves are brought to intersect each other. The measured shock inclinations as a function of wedge angle indicate a considerable departure from a simple gasdynamic flow model. It is believed that the self-generated (reversed) magnetic field associated with the laser-produced-plasma shock greatly influences the shock behavior.

I. INTRODUCTION

When a high-power laser beam is focused onto a target, a multiply ionized plasma of target material expands at a high streaming velocity. If such a supersonic plasma flow is made to collide obliquely with a solid wall, it is found that thin, highly luminous fronts develop with only a slight or no decay in plasma temperature. In this paper it will be shown that these luminous fronts represent oblique shock waves[1] which are generated by a deflection of the plasma flow. Although a collisional shock wave produced in a steady, uniform, and neutral plasma flow with no magnetic and electric fields may, in principle, behave like a gasdynamic shock, the expanding laser-produced plasma is far more complex than an ideal flow assumed in the theory. First of all, the high-temperature plasma flow consists of a number of flow groups representing different charge states with different velocities. It is also well known[2–5] that there is a sizable magnitude of magnetic field and current associated with the laser-produced plasma. In addition, the plasma ions are not in ionization equilibrium with the ambient electron temperature, i.e., the plasma flow is in an ionization-frozen state.[6] It is of great interest, therefore, to investigate characteristics of oblique shock waves produced by such complex flow; characteristics such as the effect of the presence of highly stripped plasma ions and of multiple flow components, as well as temperature and density jumps across the shock. A systematic study of oblique shock waves which are produced over a wedge by such a highly stripped, high-temperature plasma flow has not been reported previously to the best of our knowledge.

In this study, the oblique shock waves which are generated by a laser-produced-plasma flow of carbon and lithium ions over a wedge are compared with those expected from a gasdynamic flow. It will be shown that the plasma flow produces a multiple-shock front with different shock inclinations and that each shock front represents a plasma component of a different charge state within the flow. It is also noted that the flow components of the high—charge-state plasma partially overlap in time and space. In order to differentiate between the multiple-shock fronts produced a spectroheliographic technique is utilized, which allows one to record the images in the shocked plasma of an individual flow component. The experimental arrangements including this technique are described in Sec. II. In Sec. III, the phenomenology related to the interaction of the expanding laser-produced plasma with a flat solid wall and also with a wedge is described in order to show that the observed enhanced luminosity represents an oblique shock wave. In order to determine the free-stream Mach numbers of the plasma components, the flow velocity and the local electron temperature are estimated mainly using spectroscopic methods. The shock inclinations measured as a function of wedge angle (or incident angle of a flow)

are then compared with the Mach numbers determined using gasdynamic relationships. This result is also included in Sec. III along with some features of stationary oblique shock waves produced around the wedge by the laser-produced-plasma flow. Some apparent discrepancies which exist between the experiment and what is expected from gasdynamic theory are investigated and a possible physical mechanism is considered in Sec. IV. Some of the phenomenology described in this study is probably also observed in other laser-produced-plasma experiments by previous investigators. In Sec. V, these related experiments are explained using the present results.

II. EXPERIMENTAL ARRANGEMENT

Two different Pockel-cell—switched Nd:glass lasers were used to provide a plasma flow throughout the study. The beam energy of laser A is 2.5—10 J, with a 10-ns [full width at half maximum (FWHM)] pulse duration and that of laser B is 10—20 J at 35 ns (FWHM). An aspheric lens of 30-cm focal length was used to focus the laser beam for both lasers: Laser A to a spot about 600 μm in diameter and laser B to a 150-μm-diameter spot. As will be described later, laser A was used to produce a near-cylindrical column of streaming plasma in conjunction with the wedge interaction experiment, and laser B was used to produce a conically expanding plasma for oblique interaction with a flat wall. Both laser beams produced a power density of approximately 2×10^{11} W/cm^2 at the focal spot. This value is lower than the anomalous flux-density threshold but large enough to produce fully stripped carbon and lithium ions. Both carbon and pure metallic lithium disc targets were used in this study. A polyethylene $[(CH_2)_x]$ disc was also used as a carbon target to ascertain any effect of an electrically insulating material as the laser target. The materials used for deflecting wall or wedge included electrically conducting (aluminum, tungsten-nickel alloy, and stainless steel) as well as insulating (glass and plastic) materials. The target chamber in which the target and the deflecting wall (or wedge) were contained was evacuated to a pressure of 10^{-3} to 10^{-4} Torr for most of the experiments performed unless otherwise stated.

The spectroheliography technique has been used frequently to observe spectrally resolved images of the solar disc. A similar technique was also used to record an expanding laser-produced plasma in the extreme-ultraviolet (xuv) spectral region by Doschek *et al.*[7] In the present study, a half-meter Czerny-Turner mounted spectrograph was utilized to obtain spectroheliographs of shocked plasma in the spectral region of visible and the near-uv region. This was done simply by removing the entrance slit assembly from the spectrometer and by focusing the plasma image onto a plane where the entrance slit was located using a quartz lens. Because the image magnification (at the film plane) along the dispersion direction and along the direction perpendicular to it was generally different, a calibration of angle is made whenever the wavelength or grating is changed in order to obtain shock angle from the spectroheliograph. The calibration is made directly by illuminating a wedge of known wedge angle with a mercury lamp and taking a spectroheliograph of the wedge at one of the mercury line radiations close to the spectral radiation of interest. The same spectrometer (with the entrance slit) is also used as a monochromator to measure the plasma expansion velocity with the use of photoelectric detection.

A miniature ion-charge collector was used for both the flow velocity measurement and for detecting the plasma flow behind the shock. The charge collector is similar to the one used by a previous investigator[8] and consists of a collector electrode and a 125-lines/in. copper mesh screen placed in front of it. These are built into a BNC coaxial-cable connector.

III. DEFLECTION OF A LASER-PRODUCED PLASMA AND OBLIQUE SHOCK WAVES

A. Deflection by a plane wall of a laser-produced plasma

The beam from laser B was focused onto a carbon target and a portion of the conically expanding plasma was made to collide obliquely with a plane solid wall which was parallel to the target normal and displaced 1 mm from the laser axis (see Fig. 1). The lower end of the wall is located 0.5 mm above the target surface. The incident angle of the C^{5+}-plasma flow to the wall is roughly the same as the half cone angle of the plasma expansion and is approximately 15°. Figure 1(a) shows typical spectroheliographs of the deflected plasma in C^{5+} 3434- and C^{4+} 2982-Å radiation. Notice that the spectral luminosity of the deflected plasma is many times that from the portion of (freely) expanding plasma which does not interact with the wall, and it forms a thin sheet ($\lesssim$1-mm thick) according to spectroheliographs obtained viewing perpendicular to the wall surface. The laser-produced plasma was also made to interact at an incident angle much smaller than 5° by shaping the wall. Figure 1(b) is the resulting

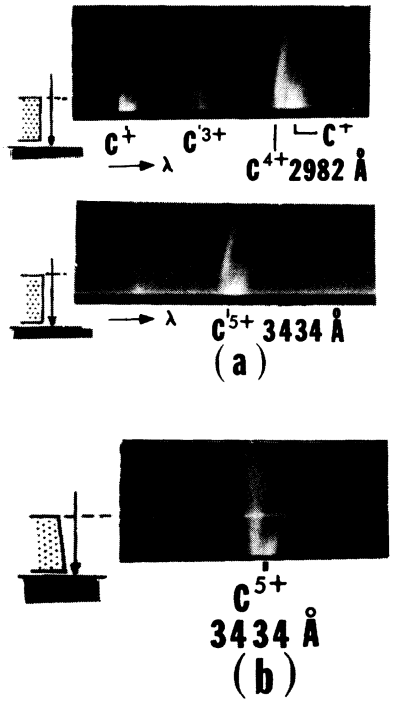

FIG. 1. Spectroheliographs of the deflected plasma in C^{5+} 3434-Å and C^{4+} 2982-Å radiation. In (a) the deflecting wall is parallel to the target normal and in (b) the wall plane makes an angle of 10° with the target normal.

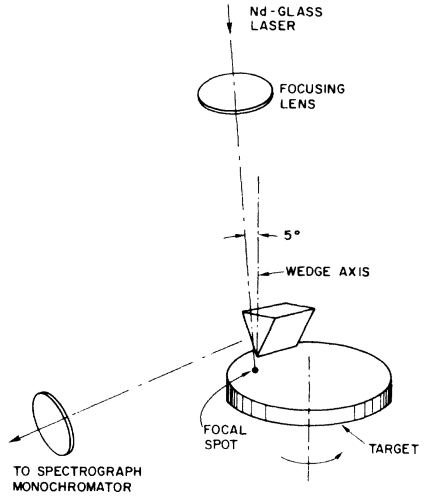

FIG. 2. Schematic diagram of laser-produced-plasma and flow-wedge interaction experiment.

spectroheliograph in C^{5+} 3434-Å radiation and one sees a marked difference between Figs. 1(a) and 1(b), i.e., in the case of Fig. 1(b) the C^{5+} 3434-Å radiation is not emitted from a well-defined thin sheet but from a broader and diffused region.

Initial experiments described above suggested that the thin plasma sheet observed in the case of Fig. 1(a) is associated with a stationary oblique shock wave produced by a supersonic plasma stream across the wall, which is similar to corner flow in the gasdynamic problem. The bright spectral luminosity observed is due to enhanced atomic transitions taking place, caused by a jump in plasma parameters across the shock (see Sec. III E). In the case of Fig. 1(b), on the other hand, it represents a weak wave or Mach wave which is a weak compressive disturbance with an infinitesimally small entropy change across the wave front.

B. Oblique shock waves around a wedge

In this subsection, the oblique shock waves which are produced by the expanding laser-produced plasma around a wedge are described. For this experiment, the beam from laser *A* is focused onto either a carbon or a metallic lithium target. A wedge is place at 3.2 mm above the target so that the expanding laser-produced plasma interacts with the wedge (see Fig. 2). Both conducting (stainless steel and aluminum) and nonconducting (machinable glass) materials were used as a wedge, but most of the data presented here were obtained with a stainless-steel wedge which is electrically grounded. The focal spot diameter of the laser beam at the target is typically 600 μm. This large focal spot size provides a relatively large-diameter plasma flow with streamlines as parallel as possible in the vicinity of wedge apex. The laser flux density is maintained at a level of 2×10^{11} W/cm^2 unless otherwise stated. The orientation of the wedge with respect to the laser beam and the target is shown in Fig. 2. In this case the incident laser is directed at an angle of about 5° with respect to the target normal. The wedge axis is parallel to the target normal, and the closest distance between the wedge wall and the laser beam is adjusted to be 1 mm in order to prevent the laser beam from grazing the wall. Also, the laser beam is in a wedge axis-apex plane in order to assure generation of a symmetrical oblique shock wave at both sides of the wedge wall.

Figure 3 shows typical spectroheliographs of an attached oblique shock wave in C^{5+} 3434-, C^{3+} 4658-, C^{2+} 4070-, and C^{+} 4267-Å radiation. A bright streak across the entire spectrum which appears in each photograph is the continuum radiation emitted in the immediate vicinity of the wedge apex, and is possibly due to the bombardment of the apex by energetic electrons and ions. One can see a thin, well-defined luminous front developing symmetri-

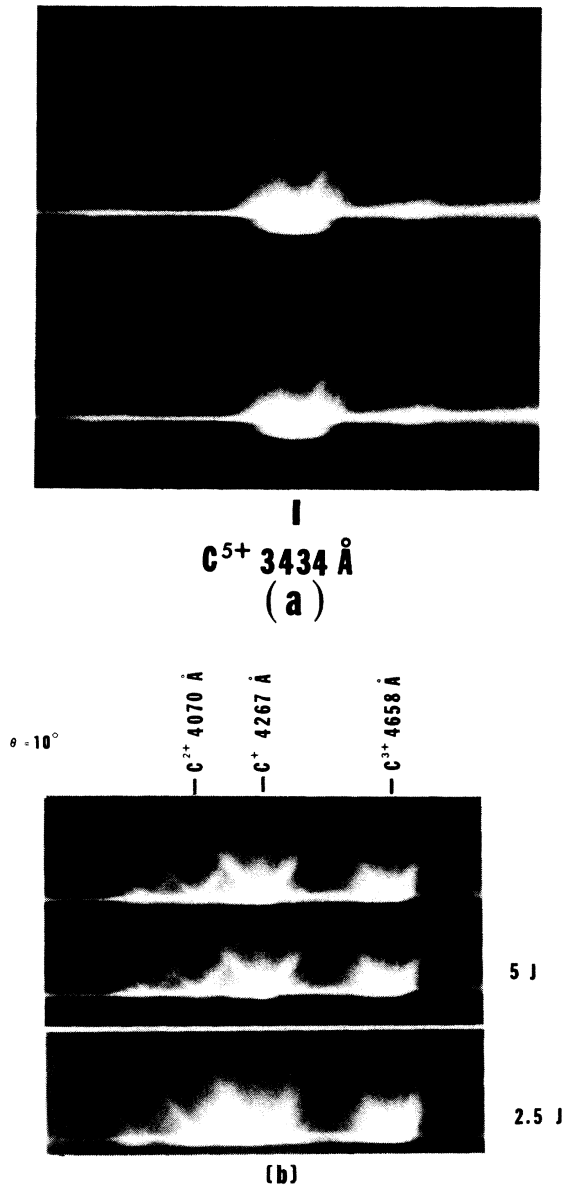

FIG. 3. Spectroheliographs of an attached oblique shock wave in (a) C^{5+} 3434- and (b) in C^{+} 4267-, C^{2+} 4070-, and C^{3+} 4658-Å radiation. In (b), two different laser energies (5 and 2.5 J) were used to demonstrate change in shock angle. $\Theta = 10°$ wedge is used for both (a) and (b).

cally with respect to the wedge axis off both sides of the wedge wall, which has different shock angles (with respect to the wedge axis) depending on the laser energy and on the ion species from which the spectral radiation originates. The thicknesses of the luminuous fronts observed in C^{5+} and C^{4+} radiation are much smaller ($<$ 1 mm) than those observed in low—charge-state spectral radiation (see Sec. III E).

Besides the attached shock front, the detached shock waves are also observed with wedges of apex half angle exceeding a critical angle Θ_{max}. Figure 4 shows an example of a detached bow shock observed in C^{2+} 2297-Å radiation at $\Theta = 10°$ and 20°. The detachment angle Θ_{max} is sensitive to the incident laser energy on the target, particularly for a low—charge-state plasma flow (or low—Mach-number flow), because Θ_{max} sensitively depends on the upstream Mach number in this case (see Sec. III C). For high—charge-state plasmas (or high—Mach-number flow), the shock detachment is not clear due to the fact that the detachment distance is small, and this small separation is further obscured by intense continuum emitted near the apex region. However, an indication of the detachment is readily detectable by apparently constant shock angles (although it must be a curved shock) which occur beyond Θ_{max}.

C. Gasdynamic oblique shock relationship

Applying the three conservation laws of mass, momentum, and energy, the relationship between the flow variables on both sides of a normal shock in a steady and uniform gas flow is given by the following equations[9,10]:

$$\rho_1 V_1 = \rho_2 V_2 , \tag{1}$$

$$P_1 + \rho_1 V_1^2 = P_2 + \rho_2 V_2^2 , \tag{2}$$

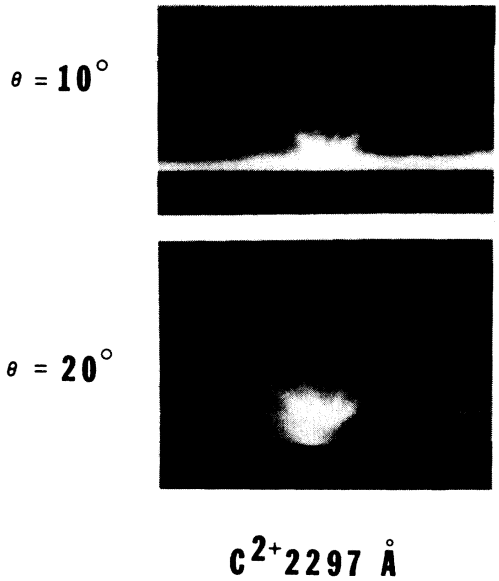

FIG. 4. Spectroheliograph in C^{2+} 2297-Å radiation, showing detached bow shock with $\Theta = 10°$ and 20° wedges.

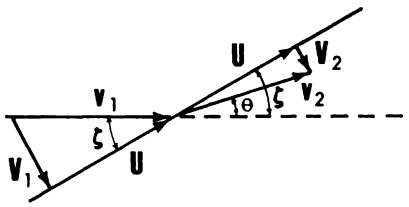

FIG. 5. Conversion from a normal shock to an oblique shock wave.

and

$$h_1+\frac{V_1^2}{2}=h_2+\frac{V_2^2}{2}\ , \tag{3}$$

where ρ, P, V, and h are, respectively, the density, pressure, flow velocity (normal to the shock front), and the specific enthalpy. The variables with the subscript 1 and 2 denote, respectively, those qualities in the front and behind the shock. The normal shock relationship shown above can be converted[9,10] into an oblique shock case by introducing the viewpoint of an observer moving with a velocity V perpendicular to the flow as shown in Fig. 5. Thus, a shock wave forms an angle ζ with respect to the upstream flow and

$$\tan\zeta=\frac{V_1}{U}\ . \tag{4}$$

The downstream flow is deflected by an angle Θ from the upstream flow and

$$\tan(\zeta-\Theta)=\frac{V_2}{U}\ . \tag{5}$$

For an ideal gas flow with constant specific-heat ratio γ, the specific enthalpy can be expressed by

$$h=\frac{\gamma}{\gamma-1}\frac{P}{\rho}\ . \tag{6}$$

The oblique shock formula which relates the shock inclination and the flow deflection in an ideal gas flow is given by[10]

$$\tan\Theta=\frac{(M_1^2\sin^2\zeta-1)\cot\zeta}{\frac{\gamma+1}{2}M_1^2-(M_1^2\sin^2\zeta-1)}\ . \tag{7}$$

The above equation represents the attached oblique shock relation. For a deflection angle greater than a certain critical angle $\Theta_{\max}$ for a given Mach number M_1, the shock front detaches from the corner (or wedge apex) and becomes the detached oblique shock. The detached shock is curved and the flow pattern behind it differs markedly from the attached shock ($\Theta<\Theta_{\max}$). There are two sets of shock angles for a given Θ according to Eq. (7); i.e., a value for ξ which is smaller than the shock angle corresponding to $\Theta_{\max}$ defines a weak shock, and a strong shock corresponds to the opposite case. The oblique shock waves which are dealt with in the present study belong to the weak shock case. For a negligibly small deflection angle Θ, $\zeta=\sin^{-1}(1/M_1)$, which represents Mach waves. The Mach-wave-like feature generated by a high–charge-state carbon plasma flow was shown in Sec. III A.

D. Flow parameters

In order to compare the present plasma result with a gasdynamic oblique shock relationship such as the one shown in Sec. III C, the flow variables of the expanding plasma should be determined. The expansion flow velocity and the electron temperature were determined in order to estimate Mach numbers for each flow component. For this experiment, laser system A with focal spot size 600 μm (2×10^{11} W/cm^2) was used throughout and no de-

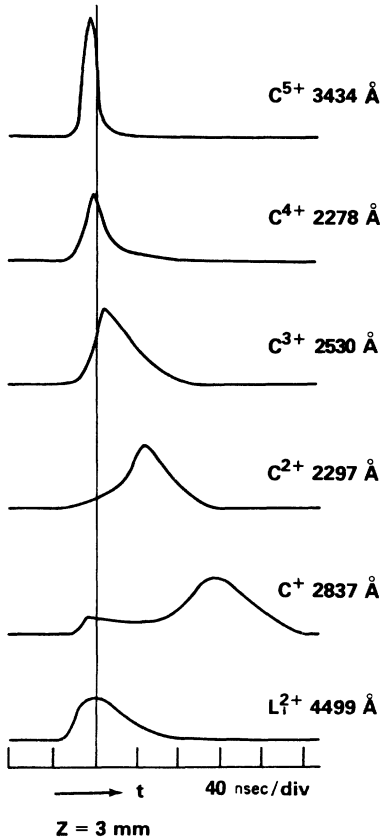

FIG. 6. Photoelectric signals of C^{5+} 3434-, C^{4+} 2278-, C^{3+} 2530-, C^{2+} 2297-, C^{+} 2837-, and Li^{2+} 4499-Å lines observed at a distance of 3 mm from the target. Entrance slit of the monochromator was oriented perpendicular to the target normal.

flecting wall was used in order to obtain the flow variables for the free expansion.

1. Flow velocity

The free expansion velocities (into vacuum) of plasma components were determined by observing spectral line signals using the monochromator-photomultiplier combination. The entrance slit of the monochromator was oriented perpendicular to the target normal so that the arrival time of spectral signal at various normal distances could be recorded. Figure 6 illustrates spectral signals of various charge-state ion species at a distance of 3 mm. Most of these spectral lines observed are from transitions between the highly excited states and generally represent[11] the ground state of the next-higher—charge-state ion. It is seen that the duration of the spectral signal gradually increases as the ion-charge state decreases. Notice also that the C^{6+}-, C^{5+}-, and C^{4+}-plasma flows closely follow each other and, in fact, partly overlap at this distance. However, as the distance increases the separation between the signal peaks widens. Each flow components named in this paper therefore is characterized by its flow velocity rather than by its constituent ion species composition, e.g., the C^{6+}-plasma component does not solely consist of C^{6+} ions but rather a mixture of other ions such as C^{5+}. The peak signal arrival is plotted versus the distance from the target surface in Fig. 7. The time of continuum peak (near 3434 Å) at the target is taken as $t=0$ in this plot. For all of the ionic species, the measured arrival times follow approximately straight lines, implying constant velocities at least

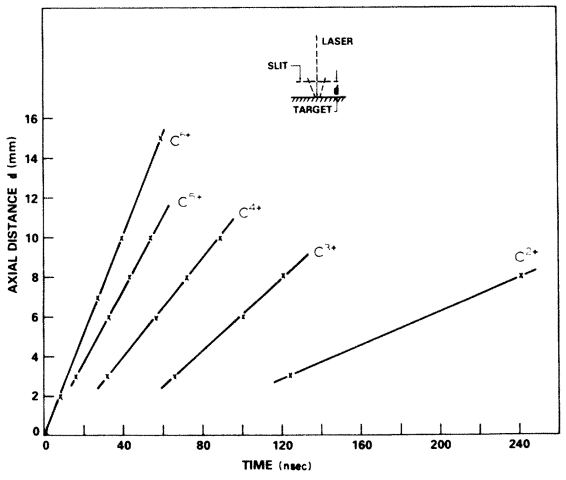

FIG. 7. Line signal arrival time vs distance from the target surface; $t=0$ corresponds to the time of continuum peak at the target.

up to 15 mm from the target. The velocities (cm/sec) obtained are, respectively, 25×10^6 for C^{6+}-, 19×10^6 for C^{5+}-, 12×10^6 for C^{4+}-, and 8×10^6 for C^{3+}-plasma flows, with an experimental uncertainty of $\pm15\%$. The expansion velocities obtained here agree well with the previous study,[12] where a carbon target with a comparable laser power density was used.

The flow velocity of C^{6+} and C^{5+} plasmas are also measured from time of flight using the ion-charge collector described in Sec. II. The velocities obtained with the ion-charge collector are in good agreement with the spectroscopically determined values within the experimental uncertainty, i.e., 26×10^6 cm/sec for C^{6+}- and 20×10^6 cm/sec for C^{5+}-plasma flows.

2. Electron temperature

The electron temperature of carbon plasmas produced from laser-irradiated solid targets has been measured by previous investigators using different techniques, and the scaling between laser flux density ϕ and the peak electron temperature at the critical density region has been reported.[13] One such scaling is given by Galanti and Peacock[14] who obtained a semiempirical relationship of $T_e\approx6\times10^{-6}\phi_A^{2/3}$ for the flux-density range of 10^{11} to 2×10^{12} W/cm^2, where $\phi_A\approx0.3\phi$ is the actually absorbed laser flux density (ϕ is the incident laser flux density). Using this relationship, $T_e\sim100$ eV at the focal spot is obtained with $\phi\approx2\times10^{11}$ W/cm^2 for the present case. The high-temperature and high—charge-state plasma then expands into vacuum. If an adiabatic expansion with an exponent of $\gamma=\frac{5}{3}$ is assumed, the electron temperature and density would fall off according to $T_e\propto d^{-2}$ and $n_e\propto d^{-3}$, where d is the distance from the focal spot. Boland *et al.*[11] who measured electron temperature and densitites of an expanding carbon laser-produced plasma obtained the results which appear to support such an adiabatic expansion. According to their results, the electron temperature at a few millimeters from the target drops to below 10 eV. A number of other previous studies[12,15–17] with comparable laser power density and a carbon or polyethylene target are also suggestive of $T_e\sim10$ ev at $d\approx3$ mm. In the present study an electron temperature of 10 eV is assumed for the C^{6+}-, C^{5+}-, and C^{4+}-plasma components[11] and for the Li^{3+},Li^{2+} plasma components at a distance of 3 mm from the target. Using an absolute spectral line intensity measurement of carbon ions, Irons[18] estimated ion population densities of the expanding laser-produced plasma at $d\approx2$ mm. Their result showed the most populous species of ions, in decreasing order, to be C^{5+} ($\sim1.2\times10^{17}$ cm^{-3}), C^{4+} ($\sim0.8\times10^{17}$ cm^{-3}), and C^{6+} ($\sim0.3\times10^{17}$

cm^{-3}). The electron temperatures of the C^{3+} ($E_i = 64.5$ eV) or lower—charge-state carbon plasma, which is well separated from the high-velocity components, drop to a much lower value[11] ($T_e \lesssim 5$ eV) than the higher—charge-state plasmas. As will be described later, an observed rapid recombination of such ions as C^{3+} and C^{2+}, which takes place even behind the shock, supports the existence of such a low-temperature plasma which is in an extreme frozen ionization state.

3. *Effective specific-heat ratio*

Since the specific heat is not a constant in the plasma flow, an effective value of it has to be determined. The effective specific-heat ratio γ is given by[19,20]

$$\gamma' \approx 1 + \frac{1}{\frac{3}{2} + \sum_{i=1}^{Z} E_i / kT_e(Z+1)} , \tag{8}$$

where $\sum_i^Z E_i$ represents the sum of ionization energies of all the ionic species involved in a flow component. γ' is that of an ideal gas (≈ 1.67) when either

$$\sum_{i=1}^{Z} E_i \gg kT_e(Z+1)$$

or a flow component consists solely of a fully stripped (e.g., C^{6+}) ion plasma. On the other hand, $\gamma' \sim 1.2$ when

$$\sum_{i=1}^{Z} E_i \approx 3.5 kT_e(Z+1) .$$

As described earlier, each flow component of the laser-produced plasma consists of two or more different charge-state ions with a certain population density distribution among them (depending on T_e and N_e at the focal spot). Therefore, for the isothermal plasma components under interest, which are in an ionization frozen state, one expects[19–22] $\gamma' \approx 1.2$.

4. *Mach number*

The upstream Mach number of a plasma flow is given by

$$M_1 = \frac{v_1}{a} \approx \left[\frac{v_1^2 m_i}{kT_e(Z+1)} \right]^{1/2} , \tag{9}$$

assuming that $T_i \sim T_e$ and that charge neutrality is valid, where v_1, a, m_i, and Z are, respectively, the flow velocity, the ion sound velocity, the ion mass, and the ion-charge state. Taking the most populous charge state, i.e., $Z=5$ for the carbon plasma and $Z=3$ for the lithium plasma, the isothermal ion sound velocities are 2×10^6 cm/sec for the carbon and 2.7×10^6 cm/sec for the lithium plasma. Table I shows the ionization energies, the upstream flow velocities, the electron temperatures, the ion sound velocities, and the corresponding upstream Mach numbers for C^{6+}-, C^{5+}-, C^{4+}-, C^{3+}-, Li^{3+}-, and Li^{2+}-plasma flows. The Mach numbers are relatively insensitive to T_e (and particularly to T_i) and the uncertainty introduced by the temperature is small. By the same reason, the local ion sound velocity (and the Mach number) of a flow component does not vary noticeably over the distance of 2–6 mm from the target. The uncertainty in determining the gasdynamic Mach number $(M_1)_{GD}$ is estimated to be about $\pm 30\%$.

TABLE I. E_i, ionization energy; a, ion sound velocity; $(M_1)_{GD} = v_1/a$ $(M_1)_{\zeta\text{-}\Theta}$; Mach numbers inferred from the ζ-Θ plots. Uncertainty involved in determining higher Mach numbers ($\gtrsim 6$) from the ζ-Θ plot is considerable because the shock angle is relatively insensitive to the Mach number in this regime.

Plasma flow component	E_i (eV)	v_1 (10^6 cm/sec)	T_{e1} (eV)	a (10^6 cm/sec)	$(M_1)_{GD}$	$(M_1)_{\zeta\text{-}\Theta}$	Shock luminosity observed in
C^{6+}		25			12.5	3–$\gtrsim$6	C^{5+} 3434 Å C^{4+} 2982 Å
C^{5+}	490	19	~10	2	9.5	2.4–3	C^{3+} 2530 Å 2906 Å 4658 Å
C^{4+}	392	12			6	2.1	C^{2+} 4070 Å C^{+} 4267 Å
C^{3+}	64.5	8	~5	1.1	7.2		C^{2+} 2297 Å ?
Li^{3+}		20	~10	2.7	7.3	3.5–$\gtrsim$6	Li^{2+} 4499 Å
Li^{2+}	122.5	14			5.2		Li^{+} 4678 Å

E. Shock front and shock luminosity

Before analyzing the spectroheliographic data such as shown in Fig. 3, it is important to ascertain what this recorded luminous front really represents. One may define two different thermodynamic transition layers[23] associated with a shock front; one is the viscous shock or shock compression layer, and the other represents the relaxation region where equipartition between ions and electrons is established. Because of large ion viscous force, compared to that of electrons, it is the ions which are heated abruptly through a rapid ion-ion collision interval (τ_i) in the compression layer. The thickness of the viscous shock front is therefore of the order of $\tau_i \bar{v}_i$, where $\bar{v}_i$ is the ion thermal velocity, or of the order of the Coulomb mean free path of the ions,[24,25] i.e., in cm,

$$\lambda_i \sim 6\times 10^{13} T_i^2/Z^4 N_i \ln\Lambda \ . \tag{10}$$

Taking $Z=5$ for C^{5+} plasma, $T_i \sim 30$ eV, and $N_i \sim 10^{16}$ cm^{-3}, λ_i becomes 6×10^{-4} cm. The thickness of the luminous fronts observed in C^{5+} and C^{4+} line radiation are of the order of 10^{-2} cm. Noting the Z^{-4} dependence on λ_i, it is also understandable why the shock luminous fronts observed in line radiation arising from lower—charge-state ions are much thicker than those from high—charge-state ions. The heating of the electron gas in the compression layer is due to an adiabatic compression, and the electron temperature is much lower than that of ions. Because the characteristic time of electron-ion collision, τ_{ei}, is much longer than τ_i by a factor of $Z^2(m_1/m_e)^{1/2}$, the equilibrium between the two groups of charged particles is slow and will be established during the declining period for T_i, at a location further from the shock compression region. The characteristic distance[25] which may be roughly $\Delta d \sim \tau_{ei} v_2$ (v_2 is the flow velocity at behind the shock) is much greater than 10 cm for the carbon plasma in the present experiments. Therefore, the thin luminous fronts observed in the spectroheliographics clearly represent the compression shock rather than the extended relaxation region described above.

Another question which arises concerning the luminous shock front concerns what atomic transition is mainly responsible for the enhanced spectral luminosity in the compression shock layer, if it represents the viscous shock. As mentioned above, the electron temperature in this region may be determined by adiabatic compression, i.e.,

$$T_{e2}/T_{e1} \sim (N_{e2}/N_{e1})^{\gamma'-1} \ .$$

Figures 8(a) and 8(b) show the gasdynamic jump relation in ρ_2/ρ_1 (or N_{e2}/N_{e1}) and T_2/T_1 and

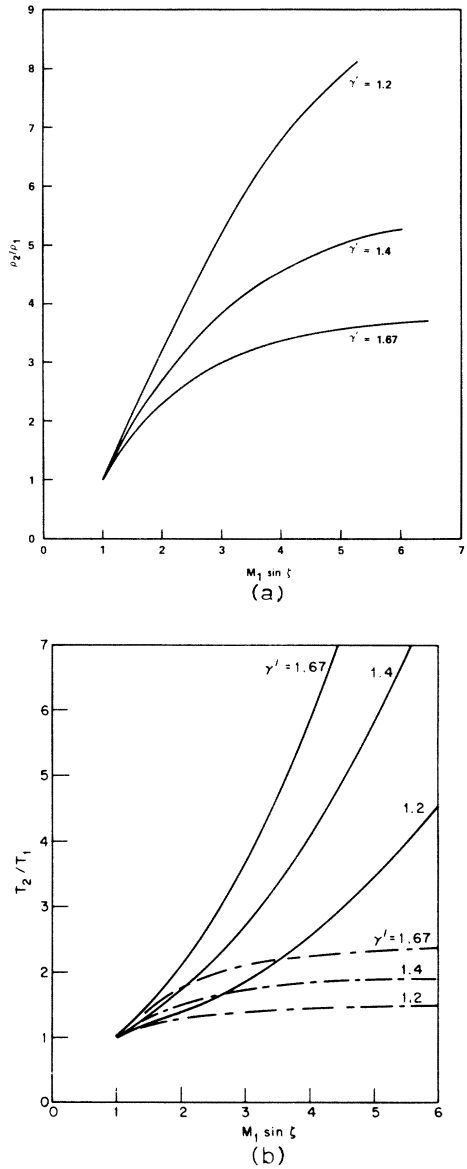

FIG. 8. Density (a) and temperature (b) ratio across an oblique shock wave as a function of $M_1 \sin\zeta$ and γ'. Electron-temperature ratio (in dashed lines) is obtained assuming an adiabatic compression.

T_{e2}/T_{e1}, respectively, as a function of oblique shock Mach number $M_1 \sin\zeta$ for three different values of γ'. Unlike T_2/T_1, the ratio T_{e2}/T_{e1} reaches a plateau (corresponding to that in ρ_2/ρ_1) at a relatively small value of $M_1 \sin\zeta$, depending on γ'. In the present experimental condition, the shock strengths are $M_1 \sin\zeta \lesssim 6$ and T_{e2}/T_{e1} is generally not greater than 1.5 in most cases for $\gamma' \sim 1.2$. Since the upstream plasma flow is already in an ionization-frozen state as is seen in Table I, the small electron-temperature jump is not likely to cause vigorous ion-

ization of such ions as C^{5+} ($E_i = 490$ eV) or C^{4+} ($E_i = 392$ eV). It is therefore likely that the shock luminosity observed in this experiment is mainly due to recombination, which is enhanced by a large electron density jump (see Fig. 8) across the shock front. This consideration is supported by the observation of line radiation arising from a lower ionization state than the upstream plasma ion component, which will be described in Sec. III F (see Table I).

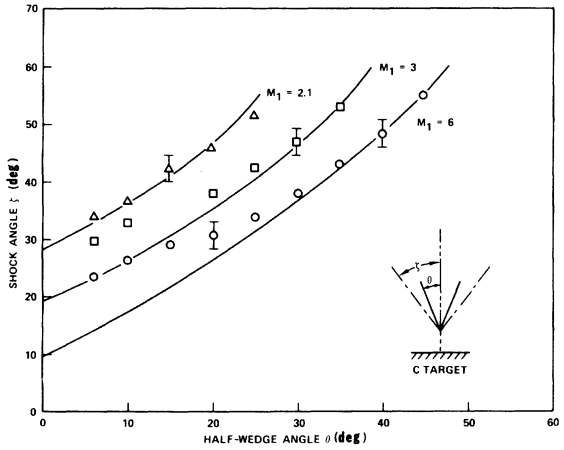

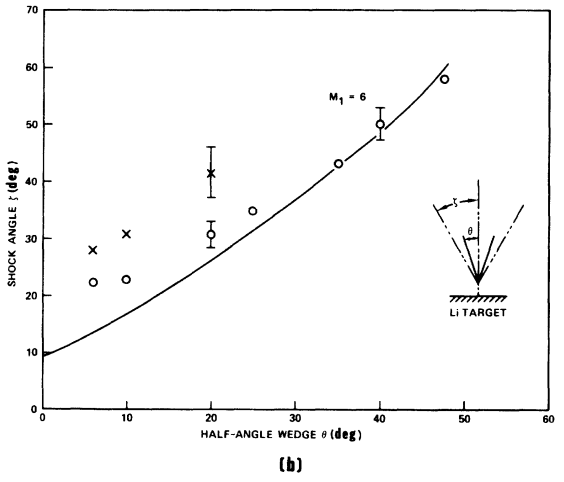

FIG. 9. (a) Shock angle ζ as a function of wedge (half) angle Θ for the carbon-plasma flow, measured from the spectroheliographs in C^{5+} 3434- (and C^{4+} 2982-) (○), C^{3+} 4658-, C^{3+} 2530- and C^{3+} 2906- (□), and C^{2+} 4070- and C^{+} 4267-Å (△) radiation. (b) Shock angle ζ as a function of wedge (half) angle Θ for the lithium-plasma flow, which is obtained from the spectroheliographs in Li^{2+} 4499- (○), and Li^{+} 4678-Å (×) radiation. Solid curves included are gasdynamic ζ-Θ plots obtained from Eq. (7).

F. Shock inclination and plasma flow behind the shock

The shock inclination can be measured from the spectroheliographs using the calibration method outlined in Sec. II. The measured shock angles depend on the wedge angle (or the incident angle of a flow to the deflecting wall), the plasma flow component (or Mach number), and the incident laser energy. The shock angle is found to be independent of the wedge material and target material [i.e., C or $(CH_2)_X$] used, whether it is a conductor or an insulator, and they are also unaffected by electrically grounding or insulating the wedge. The shock angle is also insensitive to the target-wedge apex distance within the range of ~2 to 5 mm in agreement with the T_e estimation mentioned earlier. However, the shock angles become somewhat smaller at locations closer than 1.5 mm. It is likely that the presence of the wedge in a location so close to the focal spot interferes with early expanding characteristics such as temperature. The shock angles were measured using a number of wedges with different apex angles, and these are plotted as a function of wedge half angle Θ; Figs. 9(a) and 9(b) show, respectively, the plot for the carbon- and lithium-plasma flows. The angles of the oblique shock wave observed in C^{5+} 3434 Å and C^{4+} 2892 Å are about the same within the experimental uncertainty, as are the C^{2+} 4070-Å and C^{+} 4267-Å angles. The wedge angles corresponding to the largest shock angle plotted for each group represent approximate values of Θ_{max} beyond which shock detachment occurs or the shock front disappears. A carbon-plasma shock which is represented by C^{2+} 2297-Å radiation is not included in the $\zeta-\Theta$ shown in Fig. 9(a). This shock front becomes a detached shock at as small a wedge angle as $\Theta = 10°$ (see Fig. 4), sensitively depending on the incident laser energy.

Since a multiple flow is present and a rapid recombination takes place across the shock front, it is not clear from a time-integrated spectroheliograph which upstream flow component is responsible for a shock front which is observed in a particular spectral radiation. In order to correlate each flow component with a resulting oblique shock, an ion-charge collector (probe) was utilized, i.e., the probe was used to identify the upstream components (of C^{6+}, C^{5+}, and C^{4+} plasmas) from their time of flight, since each component is characterized uniquely by its flow velocity. The probe was also used to examine the flow direction behind the shock. The directional sensitivity of the probe was improved by placing a collimator in front of the probe with an acceptance angle of 8°. The probe is movable along a circle (with a radius of 9 cm) in which the wedge apex

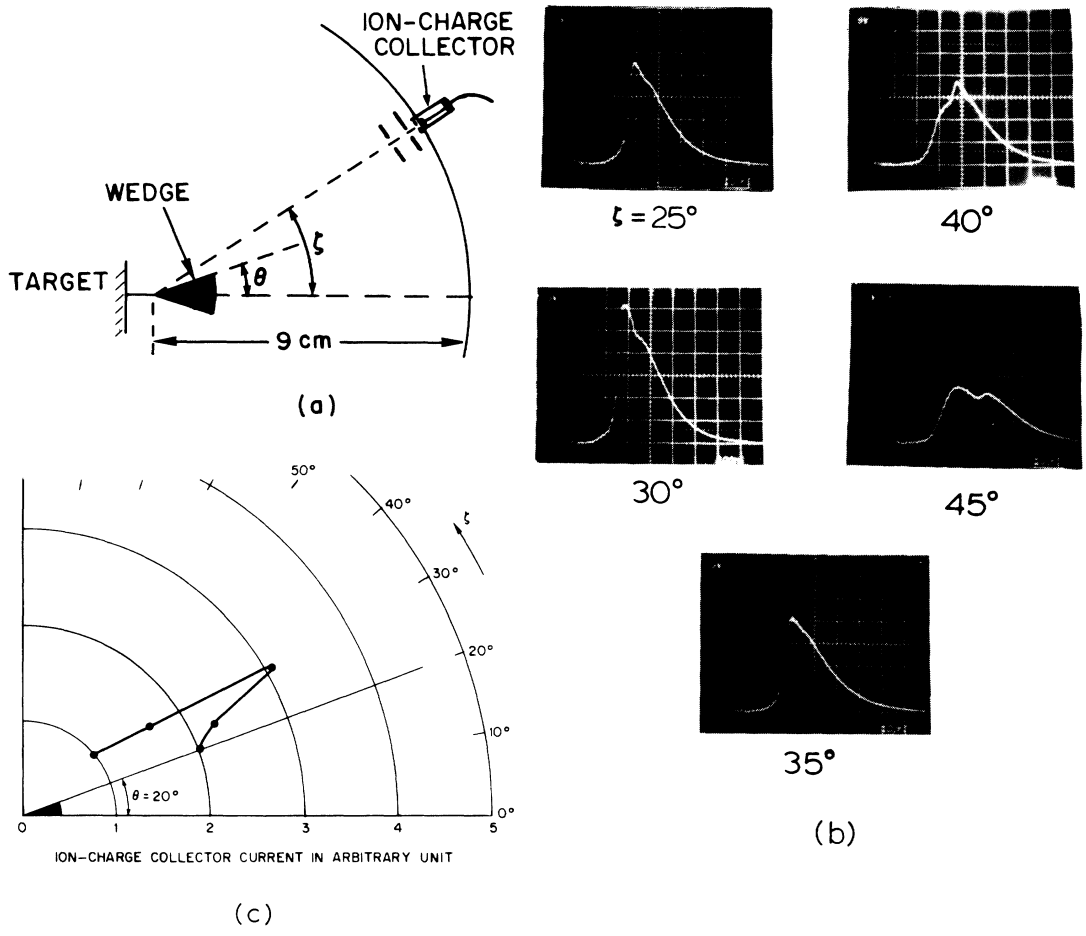

FIG. 10. (a) Experimental arrangement for angular scan of an ion-charge collector around a wedge ($\Theta = 20°$), (b) the probe signals at 5° intervals, and (c) the polar plot of probe current around the 30° region, indicating charged-particle flow parallel to the C^{6+}-plasma shock plane.

is the center, as shown in Fig. 10(a). The plane of the circle makes an angle of about 10° with respect to the wedge front face. Figure 10(b) shows the probe signals obtained from such an angular scan at 5-deg intervals using a $\Theta = 20°$ wedge. The early signal, which appears in each oscillogram, indicates the laser firing and provides a reliable time reference from which the time of flight is measured to identify the flow component. Similar probe signals are also obtained at the same angles for the free expansion case (i.e., without the wedge) for comparison. The flow signals behind the shock rise more rapidly compared with the free expansion case indicating a shock compression. It is also noted that each probe signal with the wedge is a composite of two separate signals, owing to a relatively wide acceptance angle and an existence of nonparallel flow components; one is due to a plasma flow which is deflected by the wedge wall and the other is due to a flow which is not influenced by the wedge, such as a flow which is coming directly from the focal spot. Since the latter part of the signal has the same waveform as the free expansion flow signal at the same angle, the deflected flow signal can be obtained by subtracting the latter (background) signal from the observed probe signal. The angular scan [Fig. 10(b)] then shows clear peaks at 30°, 40°, and at an angle greater than 45°. Comparing these angles with the shock inclinations measured for a $\Theta = 20°$ wedge [shown in Fig. 9(a)], the 30°, 40°, and $\gtrsim 45°$ peaks coincide, respectively, with the oblique shock observed in C^{5+} 3434-Å (and C^{4+} 2892-Å), C^{3+} 2530-Å, and C^{2+} 4070-Å radiation. The timing of these peak signals (at 9.3 cm from the focal spot) suggests that the corresponding oblique shock waves are associated with C^{6+}-, C^{5+}-, and C^{4+}-plasma (upstream) components, respectively (see Table I). This result indicates that the incident plasma rapidly recombines

across the shock front to become up to two charge states lower than the upstream flow charge state. Figure 10(c) shows a polar plot of the net ion (probe) current (arbitrary unit) as a function of scan angle ζ in the region of $\zeta=20°$ to 35°. One sees a large peak at $\zeta\approx 30°$ which corresponds to the shock front produced by a C^{6+} upstream component. The plot suggests that a predominant portion of the C^{6+}-plasma flow is transported along the shock plane rather than parallel to the wedge wall, in disagreement with the gasdynamic corner flow model (see Fig. 5). This tendency is particulary significant for the C^{6+}-plasma component and will be discussed further in Secs. IV an V.

G. Comparison with a gasdynamic oblique shock

Being able to identify the upstream flow components associated with each shock front, the measured shock angles can now be compared with those expected from the gasdynamic relationship in Eq. (7), using the Mach numbers determined earlier. The three solid curves included in Fig. 9(a) are ζ-Θ curves of the gasdynamic (GD) oblique shock which closely fit with the measured shock angles and the detachment angles. One notices that the shock angles due to the C^{4+}-plasma component [called $\zeta(C^{4+})$ hereafter] follow the GD ζ-Θ curve of $(M_1)_{\zeta\text{-}\Theta}\approx 2.1$ well with $\gamma'\approx 1.2$. For both $\zeta(C^{6+})$ and $\zeta(C^{5+})$ they seem to agree with GD ζ-Θ curves of $(M_1)_{\zeta\text{-}\Theta}\gtrsim 6$ and $(M_1)_{\zeta\text{-}\Theta}\approx 3$, respectively, with $\gamma'\approx 1.2$ for large wedge angles ($\Theta>30°$). For small wedge angles ($\Theta<30°$), however, both $\zeta(C^{6+})$ and $\zeta(C^{5+})$ deviate considerably from the GD curve. In all cases, the measured shock angles indicate much smaller $(M_1)_{\zeta\text{-}\Theta}$ by as much as a factor of 2 to 3 of the estimated gasdynamics Mach numbers (see Table I). Although there is less deviation, the similar tendency is apparent for $\zeta(Li^{3+})$ as shown in Fig. 9(b).

The plasma flow which is incident on the wedge is assumed to be a parallel flow in this study. Although a relatively large laser focal spot ($\sim 600\ \mu$m) is used to generate as parallel a flow as possible, this is obviously not the case, particularly at the periphery of the expanding plasma column. Such a nonparallel flow component tends to give somewhat smaller effective incident angle (or smaller wedge angle Θ) than the actual wedge (half) angle used. However, even if an adjustment for such a tendency is made, it would make the actual shock angle larger than the data points, which in turn makes even smaller $(M_1)_{\zeta\text{-}\Theta}$, still in a gross disagreement with the $(M_1)_{GD}$.

As mentioned earlier, the shock inclination changes according to the incident laser energy or laser power density on the target [see Fig. 3(b)], i.e., a larger beam energy tends to give a greater shock angle. This is interpreted to be related to the lower upstream Mach number (owing to a higher T_e) at the higher laser power density. Since the flow velocity of a plasma component does not decrease by increasing the laser energy, this is likely to be due to the increase in the ion sound speed. The free expansion flow velocities of C^{6+} and C^{4+} plasmas are measured using the spectroscopic method by varying the incident laser energy from 2.5 to 5 J. This result indicates that the flow velocity is not particularly sensitive to the laser energy within the energy range used and that the velocity variation is about the same as the uncertainty of the velocity measurement (15%). The shock angles $\zeta(C^{6+})$ and $\zeta(C^{4+})$ are measured by varying the laser energy, and these angles are plotted as a function of laser power density at the focal spot [see Fig. 11]. If one assumes that the local electron temperature ahead of the shock T_{e1} is proportional to that at the focal spot within the power density range used, then $M_1\propto\phi^{-1/3}$, since $T_{e1}\propto\phi^{2/3}$ and $M_1\propto(T_{e1})^{-1/2}$. The solid curves included in Fig. 11 represent the shock angles expected for a plasma flow with $M_1\propto\phi^{-1/3}$ and $\gamma'=1.2$, which is normalized to the measured angle at $\phi=2\times 10^{11}$ W/cm^2. One finds a reasonable agreement between the solid curves and the experimental values for the $\zeta(C^{4+})$-ϕ plot. In the case of the $\zeta(C^{6+})$-ϕ plot, the data points seem to vary a little or nearly stay constant over the range of power density used.

H. Magnetic field associated with shock waves

It is of interest to know of the current paths and the associated magnetic fields in the presence of the expanding laser-produced plasma, the shock wave, and the wedge. A magnetic probe of 1 mm in diam-

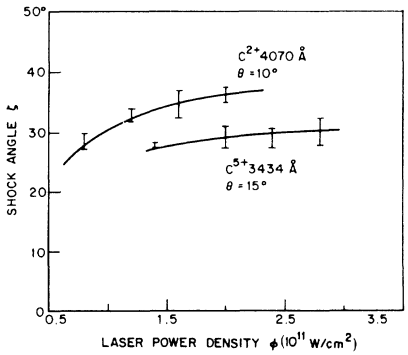

FIG. 11. $\zeta(C^{6+})$ and $\zeta(C^{4+})$ as a function of incident laser power density. Two solid curves included are obtained from Eq. (7) assuming $M_1\propto\phi^{-1/3}$ and $\gamma'=1.2$. Shock angles are normalized to the measured angles at $\phi=2\times 10^{11}$ W/cm^2.

eter and 15 turns is used to examine the magnetic field near the shock wave. The physical size (2.5-mm-o.d. glass tube) of the probe prevents the mapping of the field close to the wedge and apex region and in the vicinity of the individual shock fronts. It is also noted that the probe itself produces bow shocks by the plasma flow. Figures 12(a) and 12(b) show typical probe signals when the probe is placed 20 mm from the wedge apex: (a) right against the wedge wall and (b) 10 mm from the wall. One sees that the signal polarity changes across the shock front (in this case probably across C^{6+}- and C^{5+}-plasma shocks). The direction (conventional) of the current flow is found to point towards the wedge apex and from there presumably to the target and partly to the wedge itself, which is grounded. The wedge wall is generally covered by a boundary layer of plasma consisting mainly of C^{2+} and C^{+}. In the case of a glass wedge, the layer includes bright luminosity arising from ionized silicon atoms according to the spectroheliograms obtained. This may be taken as evidence that a current path is also provided along the wedge wall to a support which is grounded, in the case of an insulating wedge. A similar return current along a long insulating support has been previously[26] observed in laser-produced plasma. If this is the case, the magnetic field (and the magnetic pressure) behind the innermost shock (C^{6+}- and Li^{3+}-plasma shocks) must be significant, particularly near the apex region (the magnetic field in this region must be large although the field has not been measured owing to the probe size). The flow parameters (including the magnetic field) in this small region determine the shock behavior because the lateral dimension of the flow is only 3 to 4 mm at the apex and also because of a strong flow component along the shock.

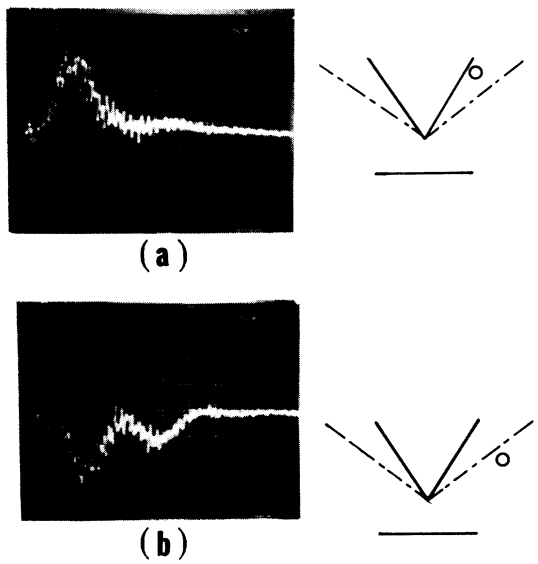

FIG. 12. Magnetic probe signal across the shock front: (a) The signal when the probe is placed right against the wedge wall 20 mm from the apex and (b) 10 mm from the wedge wall.

Since no external magnetic field is applied in this experiment, the magnetic field and the current path described above should be understood in terms of the self-generated magnetic field[2–5] associated with the laser-produced plasma. Bird *et al.*[3] reported a significant field reversal, which is observed when an expanding laser-produced plasma impinges onto a flat glass wall. Since this is apparently related to a normal shock ($\zeta=90°$) formed in the front of the wall, a similar field reversal is also expected in the case of the oblique shock wave under interest. The magnetic fields generated are due to

$$\frac{\partial \vec{B}}{\partial t}=\frac{k}{e}\vec{\nabla}_{||}T_{e2}\times\frac{1}{N_{e2}}\vec{\nabla}_{\perp}N_{e2} \tag{11}$$

and

$$\frac{\partial \vec{B}}{\partial t}=\frac{k}{e}\vec{\nabla}_{\perp}T_{e2}\times\frac{1}{N_{e2}}\vec{\nabla}_{||}N_{e2}\,, \tag{12}$$

where $\vec{\nabla}_{||}$ and $\vec{\nabla}_{\perp}$ denote the gradient parallel to and perpendicular to the shock plane. The magnetic fields generated by these two combinations of the orthogonal temperature and density gradient are opposite each other in direction and both fields are strongly dependent on the density gradient term. The $(1/N_{e2})\vec{\nabla}_{\perp}N_{e2}$ of Eq. (11) is significant in front of the shock and the direction of the field generated is such that it weakens[3] or cancels the initial field (the field due to the free expanding plasma) ahead of the shock. The reversed magnetic field generated behind the shock is believed to be owing to the $\vec{\nabla}_{\perp}T_{e2}$ [in Eq. (12)] near the wedge apex region

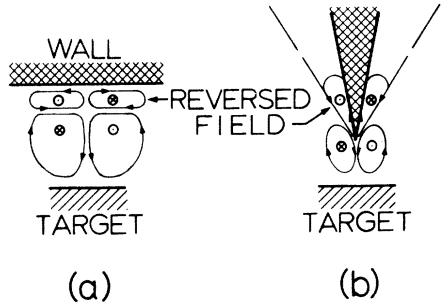

FIG. 13. (a) Self-generated and reversed magnetic fields, and associated current loops in the case of a normal shock ($\zeta=90°$) in the front of a glass wall and (b) of an attached oblique shock wave around a wedge (nonconducting material).

where the shocked plasma is relatively close to the (cold) wegde wall. Assuming that the ratio N_{e2}/N_{e1} is to be constant for a given oblique shock,

$$\frac{1}{N_{e2}}\vec{\nabla}_{||}N_{e2}=\frac{1}{N_{e1}}\vec{\nabla}_{||}N_{e1}\ , \tag{13}$$

where $\vec{\nabla}_{||}N_{e1}$ is the electron density gradient parallel to the shock plane ahead of the shock. The $\vec{\nabla}_{||}N_{e1}$ will be significant when the shock angle is small, since the density gradient is steepest along the axial direction in a free expanding plasma.

Figure 13(a) shows a possible self-generated magnetic field and current path in the case of a normal shock. Since both the self-generated and the reversed magnetic fields are azimuthal,[3] the current paths associated with the reversed field will have a similar shape as the current loops due to the nonreversed field. It is, however, considerably flattened, and one side of the current loop is parallel to the shock front while the other side is parallel to the wall surface. Similar configurations of the field and current loop are expected for the oblique shock case as indicated in Fig. 13(b), which is in agreement with what was described earlier. Note the current path along the wedge wall (insulating wedge case) and a possible loop connecting this current path to the current sheet associated with the shock front.

IV. DISCUSSION

Although a simple gasdynamic shock relationship such as Eq. (7) is compared with the experimental results, it is obvious that such idealized conditions assumed do not prevail in the present case. The discrepancy which exists in the ζ-Θ plots (shown in Fig. 9) is therefore believed to be caused mainly by such factors as the presence of multiple components in the flow and the self-generated magnetic field. A comprehensive analysis of the oblique shock wave which includes all of these effects is complex and has not been attempted here; instead, some considerations are made to offer a qualitative explanation to the experimental results.

For a given wedge half angle Θ, the shock angle ζ is a function of upstream Mach number M_1 and the effective specific-heat ratio γ' according to Eq. (7); i.e., the smaller the M_1 the larger the shock angle ζ results and the larger values of γ' tend to give somewhat larger ζ. For instance, in order to satisfy the measured $\zeta(C^{6+})$ for $\Theta=10°$, the $M_1-\gamma'$ combination should be somewhere between $M_1\sim 3$ with $\gamma'\sim 1.2$ to $M_1\sim 3.5$ with $\gamma'\sim 1.67$. In any case, the lower effective Mach numbers are needed to explain the experimental shock angle. The lower values of M_1 are not likely to be due to a larger ion sound speed in the flow because this requires a local electron temperature of as much as ten times (~ 100 eV) that which is estimated ($T_{e1}\sim 10$ eV).

The lower effective Mach number may result when a magnetic field of $(B^2/8\pi N_e kT_e)\gtrsim 1$ is present in the plasma flow, since the magnetosonic contribution becomes significant in this case. A number of previous investigators have made detailed analytical studies[27–30] of an oblique shock around a wedge (nonconducting material) produced by a magnetohydrodynamic (MHD) flow under the presence of a uniform externally applied magnetic field. However, these analyses do not apply to the present case because the magnetic field observed in this experiment is not an externally applied one but is rather associated with the current itself, which is inherent to the expanding laser-produced plasma. The magnetic field reverses its sign across the shock front in the present case.

As described ealier, multiple plasma flows are present which are partly overlapping each other. These flows produce three or more separated shock fronts in the case of the carbon plasma, the innermost shock front being due to the C^{6+}-plasma component, i.e., $\zeta(C^{6+})<\zeta(C^{5+})<\zeta(C^{4+})$. Since these shock fronts carry current and a large portion of the return current (see Sec. III H) takes a path to the wedge or along the wedge wall, the innermost shock front [$\zeta(C^{6+})$ or $\zeta(Li^{3+})$] is under a strong influence of $\vec{j}\times\vec{B}$ force which is directed outward. The shock angle will increase until the magnetic pressure balances the kinetic pressure p_2 of the shocked plasma according to the snowplow model.[31,32] The pressure ratio p_2/p_1 across an attached shock increases rapidly with $M_1\sin\zeta$ and therefore the influence of the $\vec{j}\times\vec{B}$ force will be greater for small shock angles for a given M_1. However, the influence of the $\vec{j}\times\vec{B}$ force becomes less important for larger shock angles probably because the $\vec{j}\times\vec{B}$ force does not increase as rapidly as p_2 as the shock angle increases. This explantion is in good qualitative agreement with the experimental $\zeta(C^{6+})$-Θ plot described in Sec. III.

The $\vec{j}\times\vec{B}$ force exerted onto the current sheet decreases rapidly along the shock front as the distance from the wedge apex increases due to a decrease in the magnetic field. This is the case for p_2, since p_1 decreases rapidly (at least $p\propto d^{-3}$ in the present case) as the distance from the focal spot increases. Assuming the pressure ratio p_2/p_1 for a given oblique shock is constant along the shock front, the pressure gradient $\vec{\nabla}_{||}p_2$ is given by

$$\vec{\nabla}_{||}p_2=\frac{p_2}{p_1}\vec{\nabla}_{||}p_1\ , \tag{14}$$

where $\vec{\nabla}_{||}p_1$ is the pressure gradient parallel to the shock front, ahead of the shock. Since p_2 is bal-

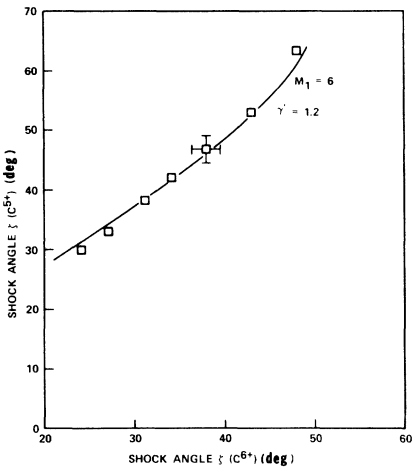

FIG. 14. $\zeta(C^{5+})$ as a function of $\zeta(C^{6+})$.

anced by the magnetic pressure and there is a large pressure gradient along the shock front as is shown in Eq. (14), one would expect a considerable flow component which is parallel to the shock front (see Sec. V). This plasma particle flow is believed to be responsible for the ion-charge collector data described earlier [see Fig. 10(c) and Sec. V].

If the C^{5+}-plasma shock results from the deflection of its flow which largely overlaps with the C^{6+}-plasma flow by the wedge wall (disregarding the magnetic field) then the deflected flow will be incident on the C^{6+}-plasma shock at an angle of Θ and the flow will not experience the second compression (or entropy change). It is more likely that the C^{5+}-plasma flow is influenced directly by the innermost shock rather than by the wedge wall. The C^{5+}-plasma flow is believed to be deflected by the innermost shock front because of the effective snowplowing, i.e., the innermost shock front acts as if it were a wedge itself to the following low—Mach-number flow. In order to examine this possibility, the shock angle $\zeta(C^{5+})$ is plotted in Fig. 14 as a function of $\zeta(C^{6+})$ (instead of the wedge angle). The solid curve included in the figure represents a GD curve with $M_1 \gtrsim 6$ and $\gamma' = 1.2$. One finds that the data points seem to follow the curve well and the Mach number thus inferred is in approximate agreement with the $(M_1)_{GD}$. The evidence that the C^{5+}-plasma flow does not penetrate the innermost shock is also seen in the ion-charge collector signal as is shown in Fig. 10(b), i.e., no (signal) component corresponding to the C^{5+}-plasma flow is detected at scan angles smaller than $\zeta(C^{6+})$.

The C^{4+}-plasma flow may be affected by both the C^{5+}- and C^{6+}-plasma shocks. However, a similar relationship which exists between $\zeta(C^{5+})$ and $\zeta(C^{6+})$, as shown in Fig. 14, is not expected between $\zeta(C^{4+})$ and $\zeta(C^{5+})$ because the ζC^{5+}-plasma shock does not snowplow the following flow. A plot of $\zeta(C^{4+})$ and $\zeta(C^{6+})$ showed that the data points roughly follow a GD curve with $M_1 \gtrsim 6$ and $\gamma' \sim 1.4$. So far a conclusive understanding of the C^{4+}-plasma flow and its shock wave remains to be developed.

V. RELATED PHENOMENA

It has been reported[33] that an expanding laser-produced plasma can be guided to a shape of a thin ($\lesssim 1$ mm) sheet of plasma up to a distance of more than 10 mm from the target using a pair of parallel walls (or a guiding channel). Judging from the ex-

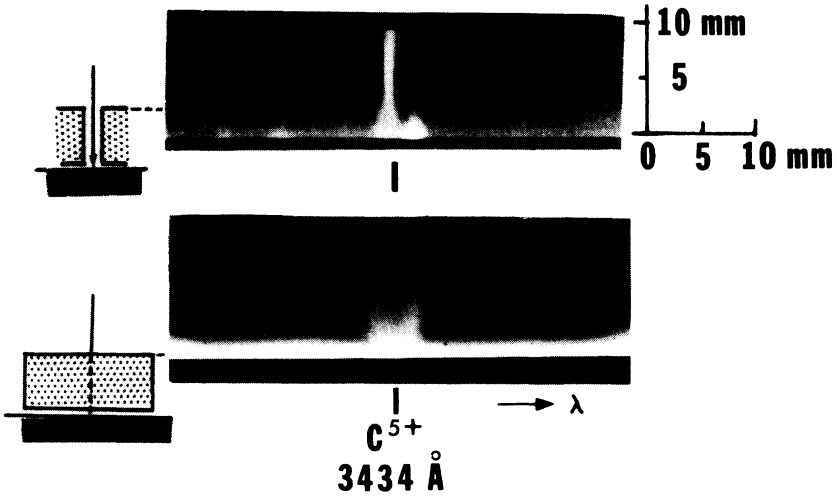

FIG. 15. Spectroheliographs of two obliquely intersecting shock fronts, in C^{5+} 3434-Å radiation obtained using a guiding channel (2-mm wide, 5 mm in height), (a) viewed along the channel, and (b) across the channel.

periment with a single wall described in Sec. III A, it is quite conceivable that the plasma collimation previously observed could be related to the interaction of two oblique shock waves which are generated by the two facing walls, respectively. Figure 15 illustrates a spectroheliograph in C^{5+} 3434-Å radiation guided by a channel of 2-mm gap with 12-mm wide and 5-mm high metallic walls, viewed along (a) and across (b) the channel. One finds that the plasma has a shape of a fan and that the plasma thickness just beyond the channel top is significantly less (≈ 1 mm) than the channel width and remains collimated ($\lesssim 2$ mm) as far as 15 mm from the target surface, in agreement with the previous result.[33] The spectral intensity of C^{5+} 3434-Å radiation beyond the channel top exceeds by many times that measured without the channel, i.e., in the case of free expansion. An examination of the spectroheliographs obtained clearly shows an oblique interaction of two luminous fronts which originate from the opposing walls.

Electron densities of the intersecting plasma and those of the free expanding plasma (without the guiding channel walls) are compared in order to see any charged-particle cumulation in the former case. This is done by measuring the Stark width of the C^{5+} 3434-Å line, which is determined from space-resolved photographic recording of this line. The orientation of the spectrometer entrance slit is parallel to the target normal and is coincident with the midplane of the channel gap. Spatial resolution is simply obtained by placing a 0.5-mm wide slit in front of the spectrometer (3600 grooves/mm grating) entrance slit. The orientation of this 0.5-mm slit is orthogonal to the entrance slit. A portion of the linewidth attributed to the Doppler effect (mainly due to the conical plasma expansion) and the instrumental width are determined by measuring the linewidth at a distance 15 mm from the target sufficient for the Stark width to be negligible but with the plasma still expanding conically. Figure 16 shows the thus obtained Stark FWHM of the C^{5+} 3434-Å line as a function of distance from the target for both cases, i.e., with and without the guiding channel.

Until recently, no detailed calculation on the Stark line profile of the C^{5+} 3434-Å line has been available. The difficulty has stemmed from an uncertainty as to whether electron impact or ion quasistatic contribution dominates the broadening. Recently, Kepple and Griem[34] have made a comprehensive calculation of the C^{5+} 3434-Å line profile based on the ion quasistatic approximation and also taking into account the contribution from the electrom collisional broadening. Using their results, the Stark linewidths are converted into electron density assuming plasma uniformity along the line of sight and charge neutrality. Figure 17 shows the electron density as a function of distance from the target. It can be seen that the electron density

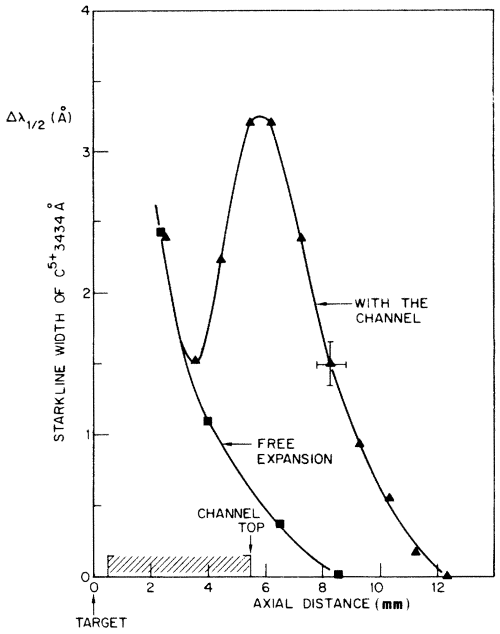

FIG. 16. Stark width (FWHM) of the C^{5+} 3434-Å line as a function of the normal distance from the target, with and without the guiding channel.

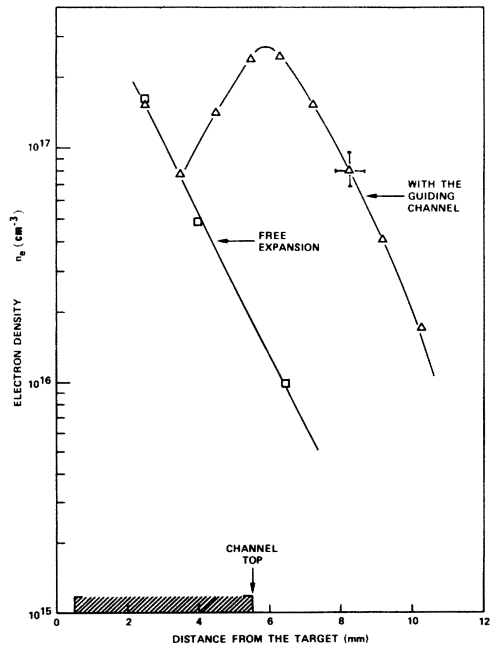

FIG. 17. Electron density as a function of distance from the target with and without the guiding channel.

begins to increase beyond the 4-mm distance from the target and peaks at about 6 mm (corresponding to 0.5 mm above the channel top) to a value greater than 10^{17} cm^{-3}. Beyond this distance the density decreases monotonically. In the case of the free expansion, the electron density decreases rapidly, in agreement with previous work.[18] Note that the electron density at the "normal" distance of 6 mm with the guiding channel is nearly 20 times greater than the free expansion case.

However, an oblique intersection of two shock waves neither necessarily brings about a flow particle cumulation nor the collimation as is seen in Fig. 17. According to the gasdynamic corner flow model, the streamlines behind an attached oblique shock wave are parallel to the deflecting wall. Therefore, the two flows deflected by the two parallel walls should also be parallel to each other and are not likely to interact [see Fig. 18(a)] to make a sheet-like collimation. The situation can be explained by the fact that a large portion of the charged-particle flow behind the shock waves are transported parallel to the shock front as shown in Fig. 18(b), in agreement with the ion probe measurement described in Sec. III F [see also Fig. 10(c)].

The plasma collimation above the channel is then reduced to the problem of two obliquely colliding plasma streams and is similar to that observed in the collapse jet[35] and the plasma jet.[36] The plasma jet is observed when a laser beam is focused onto a small conical recess made on a solid target. According to the collapse jet analysis, a jet is formed when two streams intersect at an angle greater than twice a certain critical angle $\alpha \approx \tan^{-1}(\gamma^2-1)^{1/2}$.

Conturie *et al.*[37] reported the collimation of a laser-produced plasma using a pair of thin foil ($\sim$100-μm thick) which are placed at a few hundred micrometers above the Al-target surface. The plasma collimation observed is considered to be associated with a mechanism similar to that of the guiding channel as described above. Their space-resolved x-ray spectra showed a pair of bow shocks of Al^{11+} and Al^{12+} plasma around the lower corner of each foil edge. The shock luminosity could be predominantly due to the vigorous recombination of the high-Z ions enhanced by the electron density jump across the shock front, in agreement with their results. Since the mean free path [see Eq. (10)] of the high-Z plasma ions is extremely short, a shock wave can be generated around a small object, such as the edge of a thin foil or a particle.

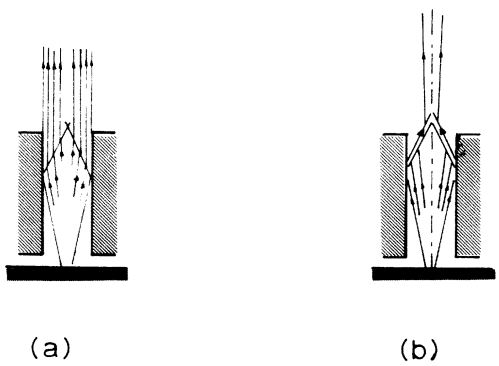

FIG. 18. Streamlines behind the obliquely intersecting shock waves, (a) streamlines parallel to the deflecting wall (possible expansion waves at the top of the wall are ignored here), and (b) streamlines parallel to the shock plane.

VI. SUMMARY AND REMARKS

When an expanding laser-produced plasma is deflected by a flat wall or a wedge, it generates Mach waves and both attached and detached oblique shock waves, depending on the incident angle and the Mach number of the flow. However, there are a number of aspects which are significantly different from what is expected from a simple, uniform gasdynamic flow. A flow of laser-produced carbon plasma, for instance, produces at least three separate oblique shock waves around a wedge, each of which are produced by a plasma component with a different velocity (and charge state) within the flow. A thin, well-defined luminosity as observed in the spectroheliograph represents a shock compression layer and is mainly associated with enhanced recombination (rather than ionization) caused by an electron density jump across the shock front. It is found that the self-generated magnetic field and the associated current greatly influence the shock behavior. A discrepancy exists between the Mach numbers determined from the experimental ζ-Θ plots and those determined from the flow velocity and the local ion sound speed. This is believed to be caused by the $\vec{j}\times\vec{B}$ force exerted onto the innermost shock front. A considerable portion of the flow particles are transported parallel to the shock front, which results in the charged-particle cumulation when two such shock waves obliquely intersect each other. This tranverse-shock[38]-like feature is caused by a steep pressure gradient parallel to the shock front and the magnetic pressure behind it. The C^{5+}-plasma flow (and also possibility the Li^{2+} plasma) is believed to be deflected by the innermost oblique shock front instead of the wedge wall. The shock inclination $\zeta(C^{5+})$ as a function of $\zeta(C^{6+})$ agrees well with that of the gasdynamic flow.

Obviously, more study is required in order to fully understand the physical picture of the oblique shock waves produced by an expanding laser-produced

plasma flow. A comprehensive analysis of the shock requires a shock relationship which takes into account the following effects: (1) The existence of a multiple flow component, (2) the self-generated (reversed) magnetic field associated with the shock front, (3) the axial and radial gradient of temperature and density in the flow, and (4) the flow of an ionization-frozen state. The spectroheliographic technique is successfully applied in order to differentiate the shock fronts produced by a multicomponent flow here. However, it fails to give time resolved information on the shock formation. Interferometry[39] using a subnanosecond laser as a light source, in addition to the spectroheliography, should yield information on more detailed aspects of the multiple-shock formation.

ACKNOWLEDGMENTS

The author would like to thank Dr. J. Y. Choe for his valuable advice and calculation on the magnetohydrodynamic oblique shock wave. He is also grateful to Dr. J. F. Seely for the helpful discussions on the electron-temperature estimation and for reading the manuscript. The author is indebted to R. L. Denningham and D. Christie for their technical assistance, and to Dr. R. C. Elton for his continued interest and encouragement. This study was supported, in part, by the U.S. Department of Energy.

[1]T. N. Lee, J. Choe, and R. L. Denningham, Bull. Am. Phys. Soc. 25, 1012 (1980).

[2]J. A. Stamper, K. Papadopoulos, R. N. Sudan, S. O. Dean, E. A. McLean, and J. M. Dawson, Phys. Rev. Lett. 26, 1012 (1971).

[3]R. S. Bird, L. L. McKee, F. Schwirzke, and A. W. Cooper, Phys. Rev. A 7, 1328 (1973).

[4]L. L. McKee, R. S. Bird, and F. Schwirzke, Phys. Rev. A 9, 1305 (1974).

[5]M. G. Droust, R. Bolton, P. Kieffer, G. Saint Hilaire, Z. Szili, H. Pepin, and B. Grek, J. Appl. Phys. 48, 2525 (1977).

[6]B. C. Boland, F. E. Irons, and R. W. P. McWhirter, J. Phys. B 1, 1180 (1968); F. E. Irons, N. J. Peacock, and R. S. Pease, Kvant. Elektron. (Moscow) 7, 20 (1972) [Sov. J. Quantum Electron. 2, 13 (1972)].

[7]G. A. Doschek, U. Feldman, P. G. Burkhalter, T. Finn, and W. A. Feibelman, J. Phys. B 10, L745 (1977).

[8]R. Decoste, NRL Memo Report No. 3774 (unpublished).

[9]Ernest Becker, *Gas Dynamics,* translated by E. L. Chu (Academic, New York, 1968).

[10]A. Owczarek, *Fundamentals of Gas Dynamics* (International Textbook, Scranton, 1964).

[11]B. C. Boland, F. E. Irons, and R. W. P. M McWhirter, J. Phys. B 1, 1180 (1968).

[12]G. V. Peregudov, M. E. Plotkin, and E. N. Ragozin, Kvant. Elektron. (Moscow) 6, 2084 (1979) [Sov. J. Quantum Electron. 9, 1224 (1979)].

[13]B. K. Sinha and N. Gopi, Appl. Phys. Lett. 35, 11 (1979).

[14]M. Galanti and N. J. Peacock, J. Phys. B 8, 2427 (1975).

[15]A. M. Malvezzi, L. Garifo, E. Janniti, P. Nicolosi, and G. Tondello, J. Phys. B 12, 1437 (1979).

[16]F. E. Irons and N. J. Peacock, J. Phys. B 7, 2084 (1974).

[17]B. A. Norton and N. J. Peacock, J. Phys. B 8, 989 (1975).

[18]F. E. Irons, J. Phys. B 6, 1562 (1973).

[19]A. Ahlborn and M. Salvat, Z. Naturforsch. Teil A 22, 260 (1967).

[20]Yu. A. Bykovskii, N. N. Degtyarenko, Y. F. Elesin, Yu. P. Kozyrev, and S. M. Sil'nov, Zh. Tekh. Fiz. 40, 2578 (1970) [Sov. Phys.—Tech. Phys. 15, 2020 (1971)].

[21]Ya. B. Zel'dovich and Yu. P. Raizer, *Physics of Shock Waves and High Temperature Hydrodynamic Phenomena,* edited by W. D. Hayes and R. F. Probstein (Academic, New York, 1966), Vol. I., p. 239.

[22]V. V. Apollonov, Yu. A. Bykovskii, N. N. Degtyarenko, V. F. Elesin, Yu. P. Kozyrev, and S. M. Sil'nov, Pis'ma Zh. Eksp. Teor. Fiz. 11, 377 (1970) [JETP Lett. 11, 252 (1970)].

[23]Ya. B. Zel'dovich and Yu. P. Raizer, *Physics of Shock Waves and High Temperature Hydrodynamic Phenomena,* edited by W. D. Hayes and R. F. Probstein (Academic, New York, 1966), Vol. II, pp. 515–522.

[24]R. A. Gross, Phys. Fluid 10, 1853 (1967).

[25]L. A. Artsimovich, *Controlled Thermonuclear Reactions,* edited by A. C. Kolb and R. S. Pease (Gordon and Breach, New York, 1964).

[26]R. F. Benjamin, G. H. McCall, and A. W. Ehler, Phys. Rev. Lett. 42, 890 (1979); P. Colodner and E. Yabolonovitch, *ibid.* 43, 1402 (1979).

[27]C. K. Chu and Y. M. Lynn, AIAA J. 1, 1062 (1963).

[28]Y. Mimura, AIAA J. 1, 2272 (1963).

[29]D. C. Pack and G. W. Swan, J. Fluid Mech. 25, 165 (1966).

[30]T. Levy, J. Mec. 7, 583 (1968).

[31]A. C. Kolb and H. R. Griem, in *Atomic and Molecular Processes,* edited by D. R. Bates (Academic, New York, 1962), Chap. 5.

[32]T. N. Lee, A. W. Ali, E. A. McLean, and A. C. Kolb, Phys. Fluids 10, 1545 (1967).

[33]J. F. Reintjes, R. H. Dixon, and R. C. Elton, Opt. Lett. 3, 40 (1978).

[34]P. C. Kepple and H. R. Griem, Phys. Rev. A 26, 484 (1982).

[35]F. H. Harlow and W. E. Pracht, Phys. Fluids 9, 1951 (1966).

[36]V. A. Gribkov, O. N. Krokhin, G. V. Sklizkov, N. P. Filippov, and T. I. Filippova, in *High Power Lasers and Laser Plasmas,* proceedings of the Lebedev Physics Institute 85, edited by N. G. Basov [Nanka, Moscow, 1976 (English translation, Consultant Bureau, New

York, 1978)], Vol. 85.
[37]Y. Conturie, B. Yaakobi, J. Delettrez, and J. M. Forsyth, *Laser Techniques for Extreme Ultraviolet Spectroscopy—Boulder, 1982,* AIP Conf. Proc. No. 1, Subseries on Optical Engineering No. 2, edited by T. J. McIlrath and R. R. Freeman (AIP, New York, 1982), p. 312.
[38]A. B. Cambel, *Plasma Physics and Magnetofluid-Mechanics* (McGraw-Hill, New York, 1963), p. 245.
[39]J. F. Reintjes, T. N. Lee, R. C. Eckardt, and R. A. Andrews, J. Appl. Phys. 47, 4457 (1976).

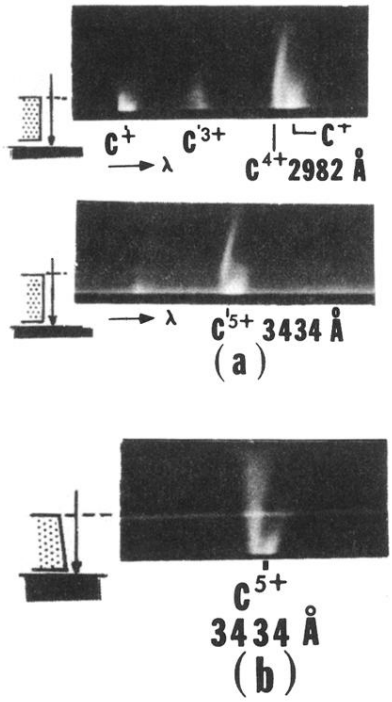

FIG. 1. Spectroheliographs of the deflected plasma in C^{5+} 3434-Å and C^{4+} 2982-Å radiation. In (a) the deflecting wall is parallel to the target normal and in (b) the wall plane makes an angle of 10° with the target normal.

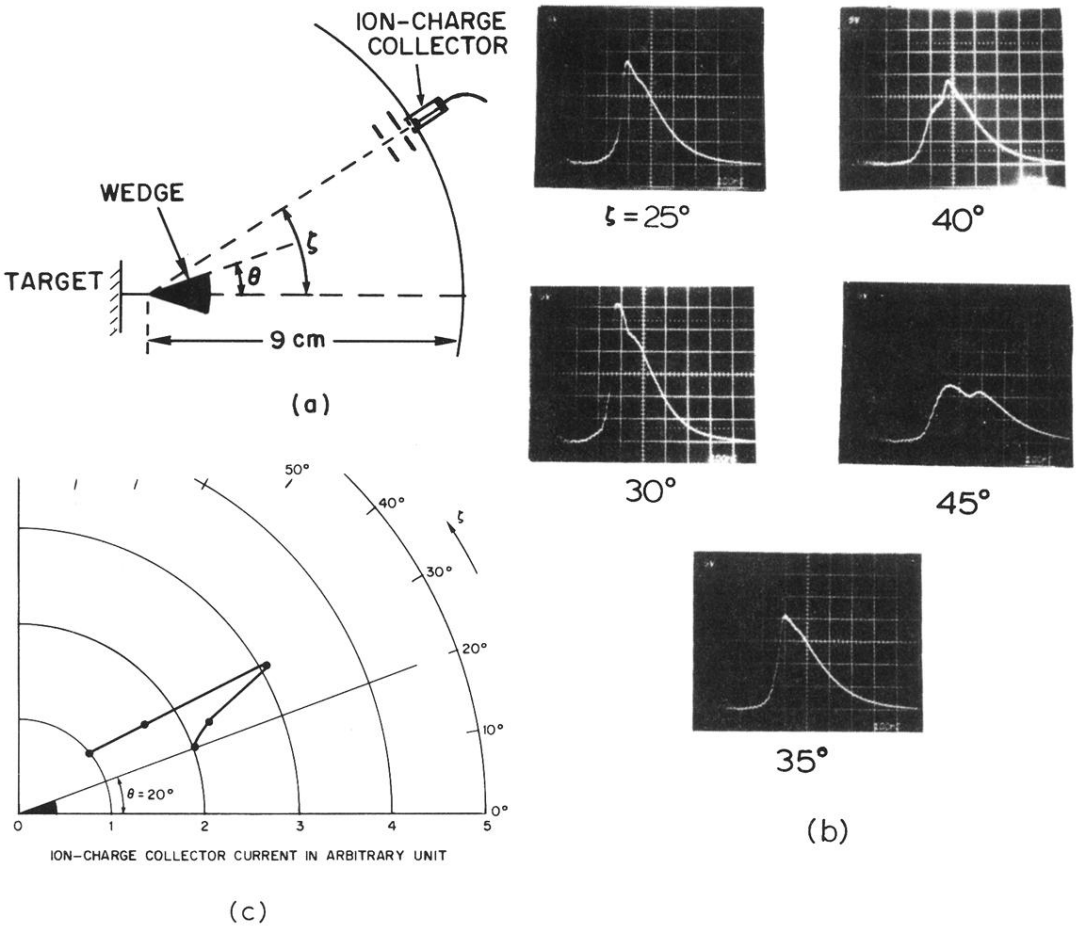

FIG. 10. (a) Experimental arrangement for angular scan of an ion-charge collector around a wedge ($\Theta = 20°$), (b) the probe signals at 5° intervals, and (c) the polar plot of probe current around the 30° region, indicating charged-particle flow parallel to the C^{6+}-plasma shock plane.

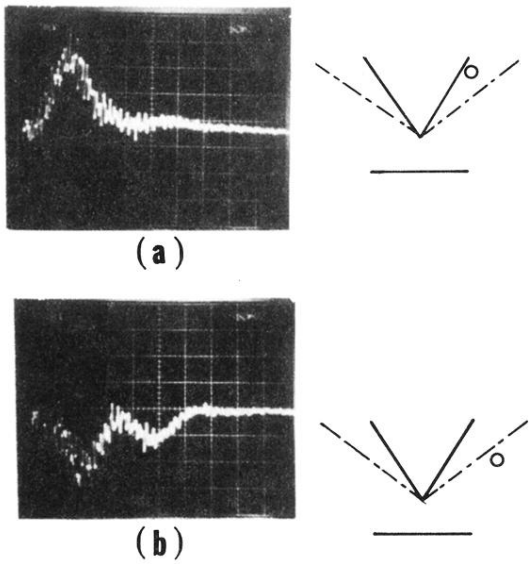

FIG. 12. Magnetic probe signal across the shock front: (a) The signal when the probe is placed right against the wedge wall 20 mm from the apex and (b) 10 mm from the wedge wall.

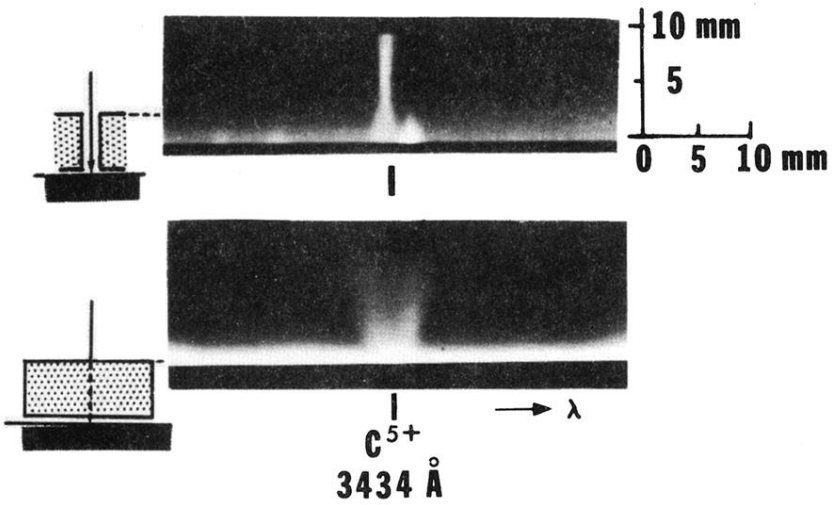

FIG. 15. Spectroheliographs of two obliquely intersecting shock fronts, in C^{5+} 3434-Å radiation obtained using a guiding channel (2-mm wide, 5 mm in height), (a) viewed along the channel, and (b) across the channel.

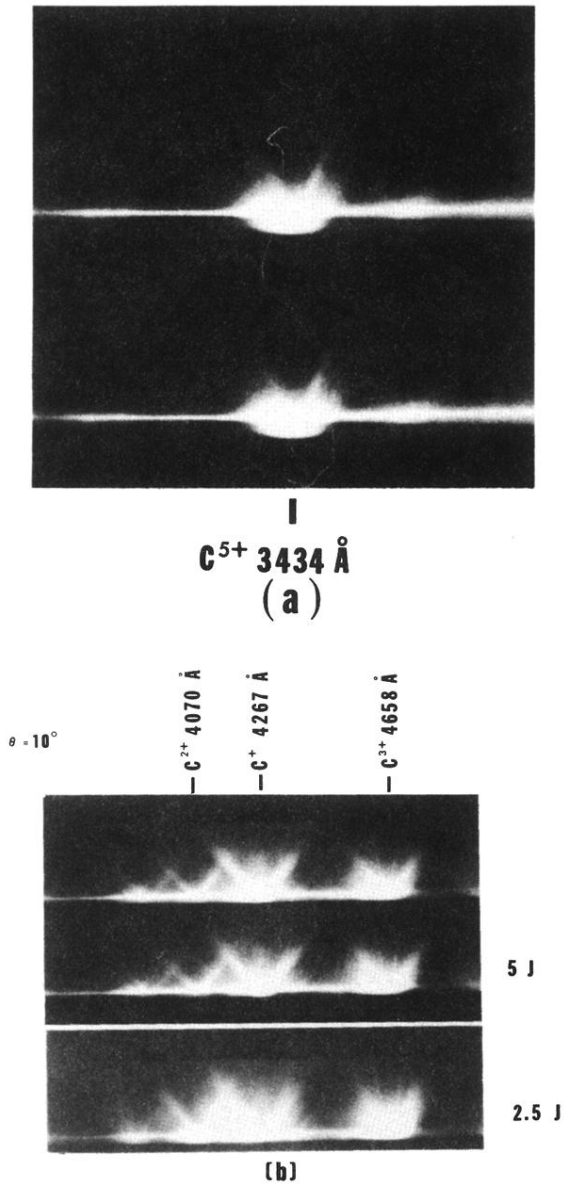

FIG. 3. Spectroheliographs of an attached oblique shock wave in (a) C^{5+} 3434- and (b) in C^{+} 4267-, C^{2+} 4070-, and C^{3+} 4658-Å radiation. In (b), two different laser energies (5 and 2.5 J) were used to demonstrate change in shock angle. $\Theta = 10°$ wedge is used for both (a) and (b).

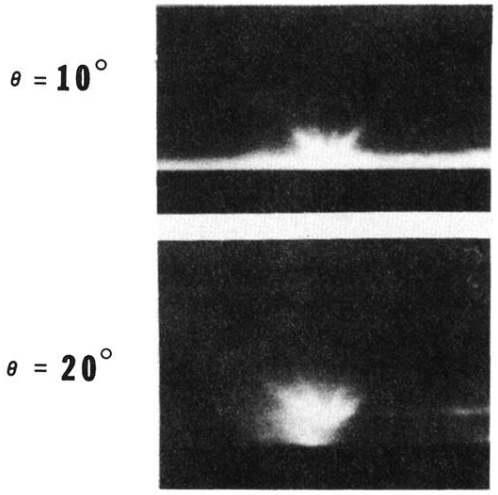

FIG. 4. Spectroheliograph in C^{2+} 2297-Å radiation, showing detached bow shock with $\Theta = 10°$ and 20° wedges.